communications materials

Article

https://doi.org/10.1038/s43246-024-00465-9

Observation of nonvolatile magneto-thermal switching in superconductors

Hiroto Arima[1], Md. Riad Kasem[1], Hossein Sepehri-Amin[2], Fuyuki Ando[2], Ken-ichi Uchida[2], Yuto Kinoshita[3], Masashi Tokunaga[3] & Yoshikazu Mizuguchi[1]

Applying a magnetic field to a solid changes its thermal-transport properties. Although such magneto-thermal-transport phenomena are usually small effects, giant magneto-thermal resistance has recently been observed in spintronic materials and superconductors, opening up new possibilities in thermal management technologies. However, the thermal conductivity conventionally changes only when a magnetic field is applied due to the absence of nonvolatility, which limits potential applications of thermal switching devices. Here, we report the observation of nonvolatile thermal switching that changes the electron thermal conductivity when a magnetic field is applied and retains the value even when the field is turned off. This unconventional magneto-thermal switching arises in commercial Sn-Pb solders and is realized by phase-separated superconducting states and resultant nonuniform magnetic flux distributions. This result confirms the versatility of the observed phenomenon and aids the development of active solid-state thermal management devices.

Thermal switching is a growing and crucial component of thermal management[1,2] because heat flow control is essential to achieve high efficiencies in electronic devices. In particular, thermal switching without mechanical motion is important to control the heat flow in solids; metal-insulator transition[3], electrochemical interactions[4], electric fields[5], and magnetic fields[6] (H) have been used to switch the thermal conductivity (κ) of materials. Magneto-thermal switching (MTS) is a promising technology because a huge MTS has been observed in spintronic multilayer films[7,8] and superconducting materials[9,10]. After investigations on various MTS materials, the MTS ratio (MTSR), which is defined as $[\kappa(H)-\kappa(0)]/\kappa(0)$, now exceeds 1000% without observation of *nonvolatile* characteristics of MTS in the superconductors. If nonvolatility with a large MTS whose $\kappa(H)$ value can be maintained at zero fields after experiencing H are obtained, they can provide a new pathway to achieve efficient thermal management in solids. In this study, we show that conventional (commercial) Sn–Pb solders exhibit a nonvolatile MTSR of 150%, which is defined as $[\kappa(0,\text{demagnetized})-\kappa(0,\text{initial})]/\kappa(0,\text{initial})$.

MTS of superconductors is achieved below its superconducting transition temperature (T_c) by forming Cooper pairs in the superconducting state, where the Cooper pairs do not transfer heat, which results in the reduction of carrier κ. The MTSR of superconductors can be extremely large; MTSR > 1000% has been confirmed in highly pure Pb[10]. This large MTSR has been achieved using the difference in electron thermal conductivity (κ_{el}) between the superconducting and normal states. Although the working temperature of superconductors is quite low, they are potentially suitable for the thermal management of low-temperature electronic devices[11,12]. However, pure superconductors do not exhibit nonvolatile characteristics related to κ_{el} in the H dependence of κ. It should be noticed that there is a report on nonvolatile MTS in a type-II superconductor Nb in the mixed states[13], and the nonvolatility is caused by the changes in the lattice thermal conductivity (κ_{lat}) in its mixed states; at higher temperatures, the fluxes also affect κ_{el}[13]. However, the nonvolatile MTS mainly based on the changes in κ_{lat} in the superconducting mixed states is highly sensitive to purity[9,13]; hence, achievement of nonvolatile MTS using the changes in κ_{el} between superconducting and normal conducting states is desired for application. In this study, we investigate the MTS characteristics of Sn–Pb solders and observe that simple solders exhibit nonvolatile MTS based on κ_{el}. We conclude that the mechanism of nonvolatile MTS in the solders is based on trapped magnetic flux, as discussed later. Flux trapping in Sn–Pb solders was investigated through magnetization measurements several decades ago[14,15], in which the Sn–Pb solders were simply regarded as type-II superconductors. However, the Sn–Pb solders are actually composite (phase-separated) materials composed of two type-I superconductors with different T_c, i.e., Sn (T_c = 3.7 K) and Pb (T_c = 7.2 K). Here, we propose that such composite superconductors trap magnetic flux nonuniformly and give rise to nonvolatile MTS.

Here, we briefly introduce the magnetic flux trapping in superconductors. Superconductors are mainly categorized into type-I and type-II,

[1]Department of Physics, Tokyo Metropolitan University, 1-1, Minami-osawa, Hachioji 192-0397, Japan. [2]National Institute for Materials Science, 1-2-1, Sengen, Tsukuba 305-0047, Japan. [3]Institute for Solid State Physics, University of Tokyo, 5-1-5, Kashiwanoha, Kashiwa 277-8581, Japan. e-mail: mizugu@tmu.ac.jp

based on the difference in their reaction to applied H[16]. In type-I superconductors, perfect diamagnetism is observed up to the critical field (H_c), and the superconducting states are quickly suppressed by applying further fields. Therefore, magnetic flux is expelled from ideal type-I superconductors in their superconducting state. Type-II superconductors have two critical fields: a lower critical field (H_{c1}) and an upper critical field (H_{c2}). At $H < H_{c1}$, perfect diamagnetism is also observed in type-II superconductors, but at $H_{c1} < H < H_{c2}$, the magnetic flux can coexist with the superconducting states. The magnetic flux inside the type-II superconductors is quantized, where the vortices with a normal-conducting core (and a lattice of vortices) are formed[16]. The observation of nonvolatile MTS based on κ_{lat} in Nb is related to this phenomenon. The vortices have been detected experimentally and investigated by various techniques[17–20]. Further, thin type-I superconductor films also exhibit vortex states when the film thickness is very thin or the films contain weak pinning centers[21,22]. Another phenomenon of trapped magnetic flux was observed in a superconductor hollow cylinder or ring[23]. Because of the shielding supercurrents in the superconducting cylinder, fluxes are trapped inside the cylinder. This phenomenon occurs in both type-I and type-II superconductor cylinders. In the solders, magnetic fluxes would be trapped in the Sn regions by this mechanism, which is achieved by shielding currents in the Pb regions. Then, the Sn regions start conducting normally (non-superconducting) because of the trapped field of $H > H_c$ (Sn). Although the mechanisms behind the flux trapping are known, unexpectedly strong flux trapping in a bulk composite composed of type-I superconductors with different T_c would provide new insights into the functionalities and applications of superconductors.

Results

Nonvolatile magneto-thermal switching in Sn–Pb solder

The most important result of this work is the observation of nonvolatile MTS based on the modification of κ_{el} in Sn–Pb solders. It is widely known that solders are phase-separated composites, but the utilization of unique superconducting states emerging in the phase-separated solders has not attracted much attention. Here, we show the nonvolatile characteristics of MTS at $T = 2.5$, 3.0, and 4.2 K as examples. The schematic images of the concept of nonvolatile MTS in solders are shown in Fig. 1. At the initial state (Fig. 1a), the whole sample is superconductive, and the κ is low due to the suppression of carrier heat transfer. At $H > H_c$, the superconducting states of the solder are totally suppressed (Fig. 1b), and κ is increased by the revival of thermal conduction by charge carriers. The nonvolatility of MTS is observed by reducing H after experiencing a large H. As shown in Fig. 1c, high κ is retained even after removing external fields (at $H = 0$ Oe), which is achieved by the magnetic fluxes trapped in the Sn regions. The nonvolatility of κ implies that several Sn grains lose the bulk nature of superconductivity and are close to normal-conducting states because of the trapped magnetic fluxes. The mechanism of nonvolatile MTS in the solder is different from that in Nb[13] where vortices modify κ_{lat}. In addition, the trapping of a large number of magnetic fluxes in the Sn regions of Sn–Pb solders had not been a common understanding in the field of pure and applied science of superconductors.

We measured the temperature and field dependences of κ for commercial Sn45–Pb55 solders using a four-probe method (Fig. 2a). Figure 2b shows the temperature dependences of κ measured at $H = 0$ Oe after zero-field cooling (ZFC) and field cooling under $H = 1500$ Oe (FC). In addition, the FC data measured at $H = 1500$ Oe are plotted together with data measured at $H = 0$ Oe (after ZFC and FC). The difference in the κ–T curve appears below 7 K, which is due to the emergence of superconductivity in the solder (at T_c for Pb; see magnetization data shown in Fig. 3a). As shown in Fig. 2b, we find that the ZFC and FC data exhibit clear differences when these measurements are performed after removing the applied magnetic field ($H = 0$ Oe) in the measurement system. At $H = 1500$ Oe (FC), the decrease in κ at low temperatures was totally suppressed because the superconducting states of the solder were destroyed. Because the FC ($H = 0$ Oe) data exhibited an intermediate trend between ZFC ($H = 0$ Oe) and FC ($H = 1500$ Oe), it is clear that magnetic fluxes, less than 1500 Oe, were trapped in the solder sample after the FC under 1500 Oe.

Figures 2c–f display the κ–H curve measured at $T = 2.5$, 3.0, 4.2, and 8.0 K. Here, error bars are not displayed for clarity, but the data with error bars are displayed in Supplementary Fig. 1. No MTS was observed at $T = 8.0$ K because the temperature was higher than T_c of the solder. At $T = 2.5$ K, a clear MTS was observed in the initial increments of H from 0 to 1700 Oe. Further, by decreasing H from 1700 to −1700 Oe, κ slightly decreases but does not reach the initial value of κ at $H = 0$ Oe. At around −800 to −1000 Oe, an anomaly is seen, which is related to the critical field (Supplementary Fig. 2). By increasing H from −1700 to 1700 Oe, a similar anomaly was observed between 800 and 1000 Oe, but the value of κ never returned to the initial value. The κ–H data clearly shows the nonvolatile MTS characteristic in the solder. The nonvolatile MTSR was about 150%, as shown in Fig. 2c. At $T = 3.0$ and 4.2 K, similar nonvolatile MTS trends were observed, while the MTSR decreased with increasing temperature. One of the reasons why nonvolatile MTS was observed at $T = 4.2$ K ($>T_c$ of Sn) would be explained by the partial suppression of the superconducting states of the Pb regions by the trapped fluxes. Another reason would be weak superconducting states in the Sn regions achieved by the proximity effects in the initial state at $T = 4.2$ K. After field experience, Meissner states cannot be achieved due to the presence of trapped fluxes. Comparable MTS

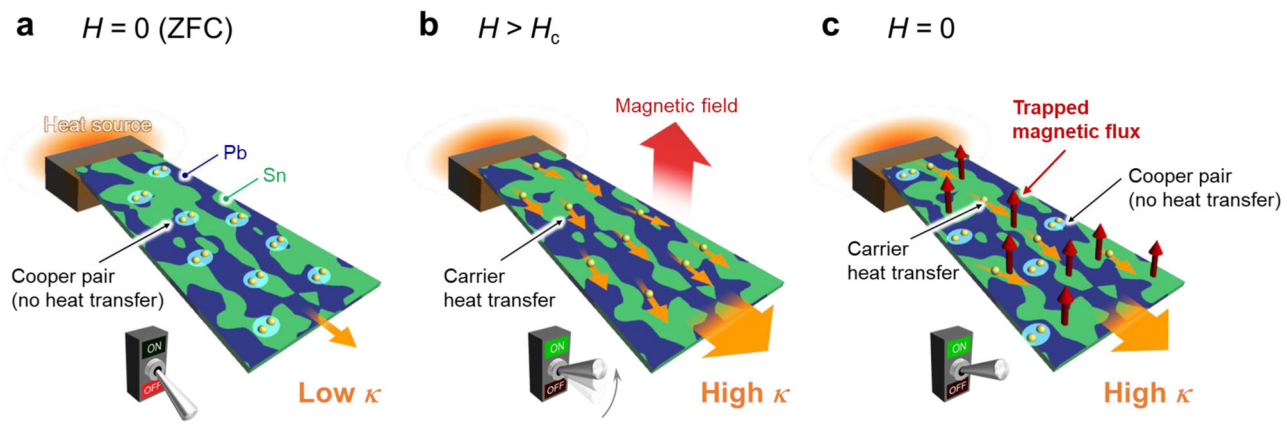

Fig. 1 | Schematic images of nonvolatile magneto-thermal switching observed in commercial solder (Sn45–Pb55). a Initial state with low thermal conductivity (κ) after zero-field cooling (ZFC). The schematic image of a switch (OFF) denotes the low-κ state. **b** State under a magnetic field (H) higher than the critical field (H_c). Magnetic field lines can penetrate whole samples because both Pb and Sn are in normal conducting states. In this state, κ is high (ON). **c** State at $H = 0$ after experiencing $H > H_c$. Pb is in the superconducting state, and the magnetic field lines do not penetrate the Pb regions. Fluxes trapped in the Sn regions cannot be released even at $H = 0$, which results in the suppression of bulk superconductivity in the Sn regions. In this state, nonvolatile MTS with high κ (ON) can be observed.

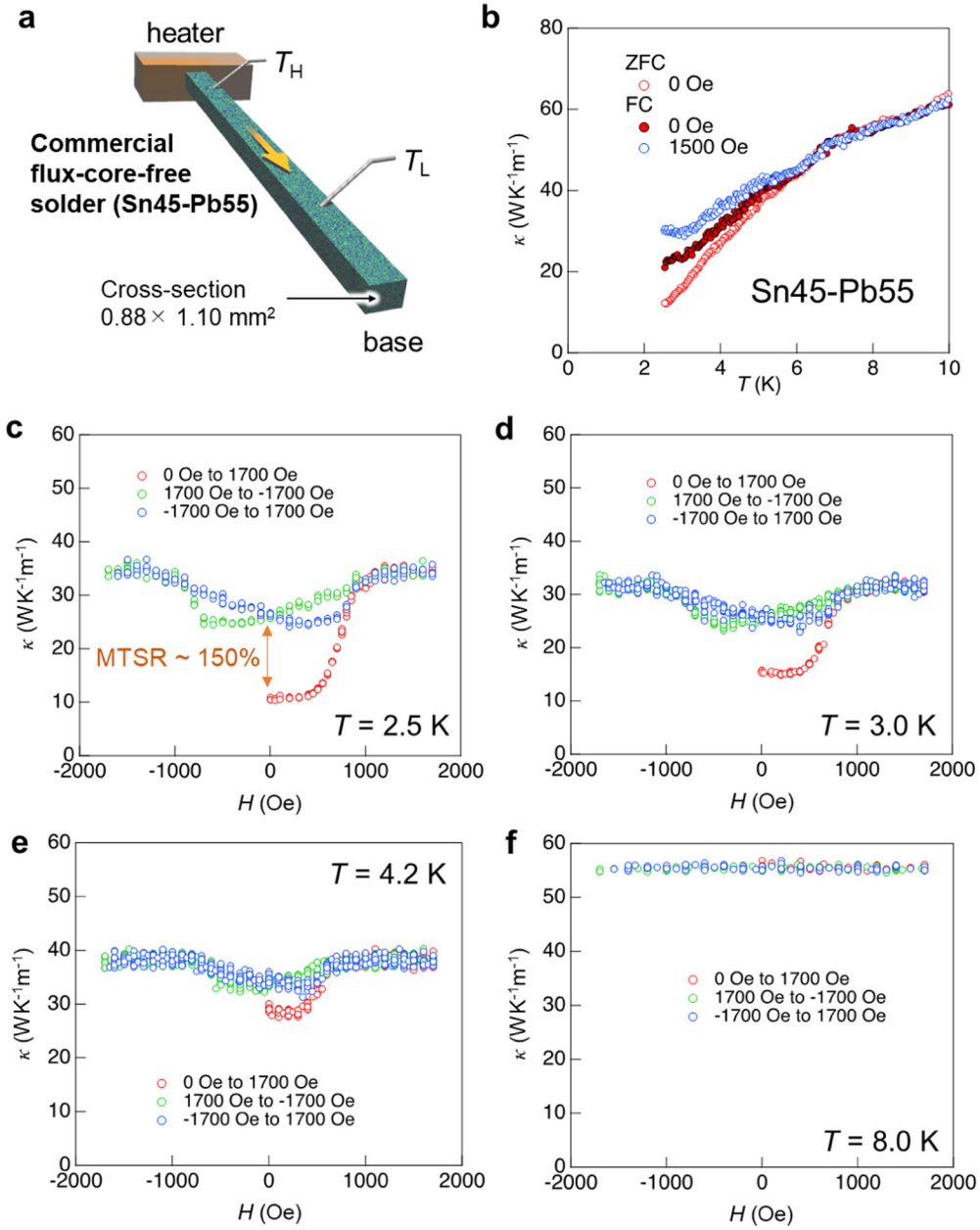

Fig. 2 | Nonvolatile magneto-thermal switching characteristics of the flux-core-free solder (Sn45–Pb55). a Schematic image of the measured sample with a cross-sectional area of 0.88×1.10 mm^2. T_H and T_L denote two thermometers. The purchased solder with a diameter of 1.6 mm was polished into a uniform rectangular bar. **b** Temperature (T) dependence of κ. The open red circles are data measured at $H = 0$ Oe after ZFC. The filled red circles are data measured at $H = 0$ Oe after field cooling under $H = 1500$ Oe: the sample was field-cooled from 10 K to 2.5 K, and the data were taken after reducing the external field. The blue open circles are data measured at $H = 1500$ Oe after FC under $H = 1500$ Oe. **c**–**f**, κ–H curves measured at $T = 2.5$, 3.0, 4.2, and 8.0 K.

characteristics were obtained for an Sn45–Pb55 solder wire in an as-purchased form with a φ1.6 mm cross-section (Supplementary Fig. 3). Furthermore, we examined the MTS on a flux-cored solder with a different composition (Sn60–Pb40) and observed similar nonvolatile MTS (Supplementary Fig. 4). Therefore, nonvolatile MTS is a common behavior in various Sn–Pb solders.

Characterization of superconducting properties and phase separation of Sn–Pb solder

To understand the causes of nonvolatile MTS in solders, the superconducting properties were investigated by measuring the magnetization (M) and specific heat (C). Figure 3a, b shows the T dependence of M measured at approximately 10 Oe after ZFC and FC (under 1500 Oe); ZFC data exhibits diamagnetism below 7.2 K, but FC data exhibits ferromagnetic-like signals below 7.2 K. Similar significant differences in the M–T between ZFC and FC have been observed in type-II superconductors; for a recent observation example, superhydrides (hydrogen-rich superconductors) exhibit similar ferromagnetic-like M–T behavior after FC[24]. This behavior is explained by the trapped flux in the type-II superconductors. In contrast, our Sn–Pb solder sample was composed of type-I Sn and Pb, which is clearly different from the former case. As shown in Fig. 4, the elemental mapping analysis revealed that there are phase-separated Sn and Pb regions with a typical size of 5–20 μm. In the μm-scale order, the superconducting states of Pb can penetrate the Sn region, which causes the single-step superconducting transition shown in Fig. 3a. Instead, the FC data in Fig. 3b exhibits a ferromagnetic-like behavior with a transition temperature of 7.2 K, which is the T_c of Pb. This suggests that magnetic fluxes were trapped in the solder at temperatures below T_c of Pb. As a

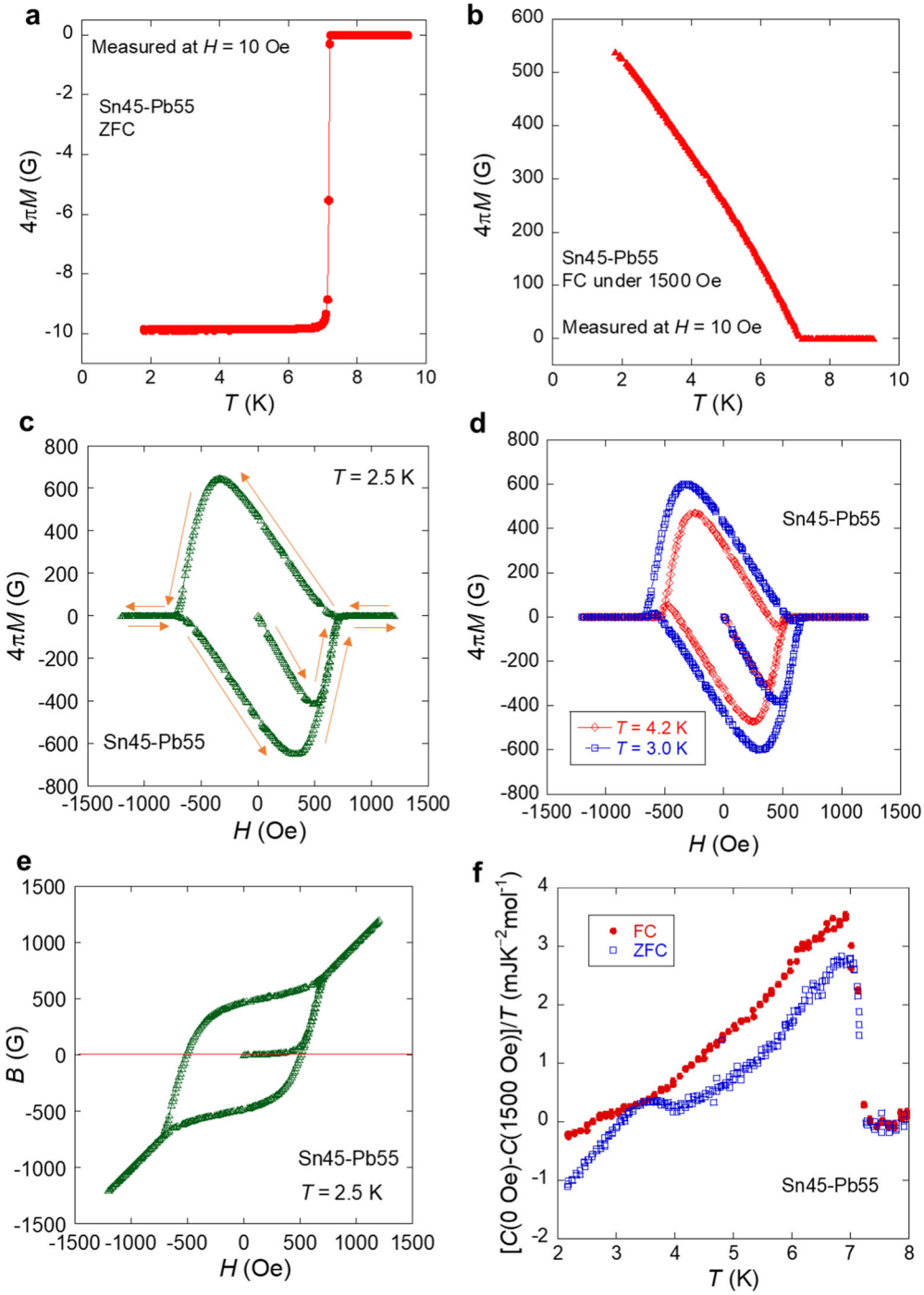

Fig. 3 | Superconducting properties of the solder Sn45–Pb55. a, **b** T dependence of magnetization ($4\pi M$) measured at about 10 Oe after zero-field cooling (ZFC) and field cooling under 1500 Oe (FC). **c**, **d** M–H curves measured at $T = 2.5$, 3.0, and 4.2 K. **e** H dependence of inner magnetic flux density (B). **f** T dependence of residual specific heat estimated by C (0 Oe) − C (1500 Oe) in the form of C/T. Both FC and ZFC data are taken at $H = 0$ Oe after FC under 1500 Oe and ZFC, respectively. The superconducting transition of Sn ($T_c = 3.7$ K) is seen in the ZFC data only.

fact, we observed the broadening of the temperature dependence of resistivity under magnetic fields (Supplementary Fig. 2). The trend is commonly observed in superconductors with magnetic flux trapping[25]. The fact suggests that the trapped fluxes are thermally fluctuating, which is consistent with the result shown in Fig. 3b.

To further characterize the magnetic properties, the H dependence of magnetization ($4\pi M$) was measured at $T = 2.5$, 3.0, and 4.2 K (Fig. 3c, d), where the data was corrected by a demagnetization factor. With decreasing temperature, the size of the $4\pi M$-H hysteresis becomes larger, which suggests the enhancement of a critical current density (J_c) and critical field. However, we noticed there was no large change between $T = 3.0$ and 4.2 K. As T_c of pure Sn is 3.7 K, the absence of a large change in the $4\pi M$–H hysteresis at around 3.7 K indicates that the characteristics of the emerging superconducting currents are governed by Pb in the solder. To further understand what is happening in the solder under magnetic fields, we plotted inner magnetic flux density (B), which is given by $B = H + 4\pi M$, in Fig. 3e. When the solder was zero-field-cooled to $T = 2.5$ K, the initial B–H curve exhibited perfect diamagnetism (Meissner states) up to about 500 Oe. Then, B becomes equal to H, which indicates the suppression of the superconducting states at $H > 700$ Oe. When decreasing the field from

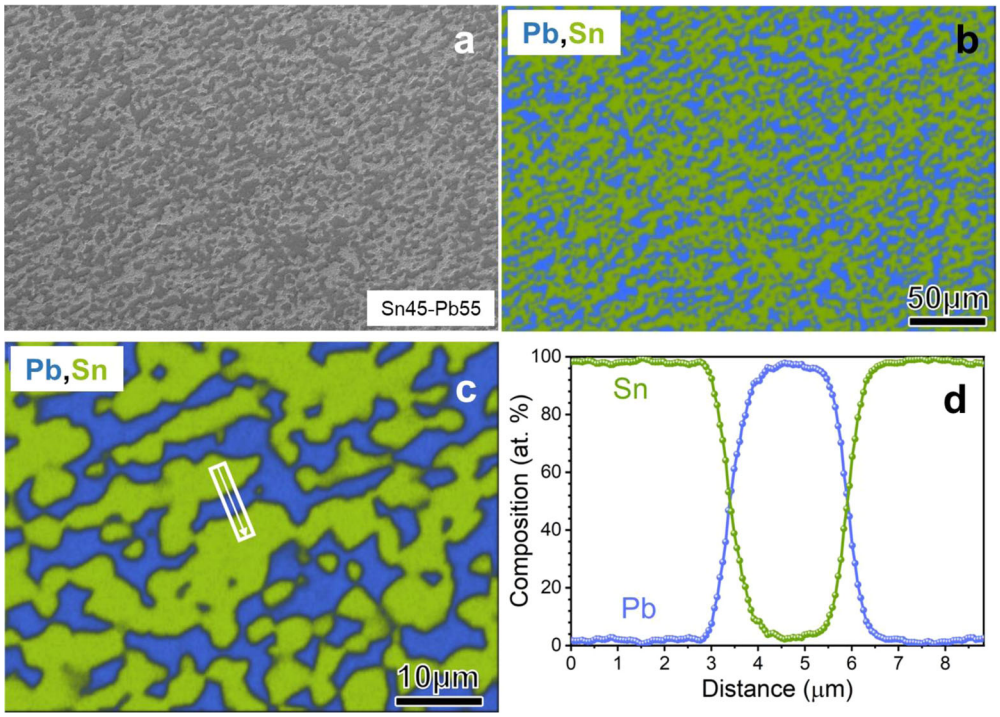

Fig. 4 | μm-scale phase separation of Pb and Sn in the solder. a Scanning-electron microscope (SEM) image on the polished surface of the solder (Sn45–Pb55). **b**, **c** Elemental mapping by energy-dispersive X-ray spectroscopy (EDX). **d** Line profiles of the compositions of Sn and Pb along the white arrow in (**c**).

$H > 1000$ Oe, an anomaly appears at $H \sim 700$ Oe, where the superconducting states of Pb emerge, and magnetic fluxes are trapped inside the solder. Even at $H = 0$ Oe, the B remains a large value of ~500 G, which is consistent with a previous work[15]. Based on those facts, we concluded that magnetic fluxes with $B \sim 500$ G can be trapped after FC or application of H greater than 700 Oe in the solder, and the flux trapping in the Sn regions is the origin of nonvolatile MTS.

To prove the assumption above, we measured the temperature dependence of zero-field specific heat (C) after ZFC and FC (under 1500 Oe). The results, including the data measured under a magnetic field ($H = 1500$ Oe), are summarized in Supplementary Fig. 5. In Fig. 3f, the C data in the form of C/T after removing normal states values, estimated by subtracting the data at 1500 Oe, are plotted as a function of temperature. As shown in Supplementary Fig. 5, from the analysis of low-temperature C at $H = 1500$ Oe using the low-temperature approximation of $C = \gamma T + \beta T^3 + \delta T^5$, Debye temperature ($\theta_D$) and electronic specific heat coefficient (γ) were estimated as 128.8(4) K and 2.14(5) mJ K^{-2} mol^{-1}, respectively. As θ_D for Pb and Sn are about 105 and 199 K[26], respectively, the obtained θ_D for the Sn45–Pb55 solder would be reasonable. For both ZFC and FC data at $H = 0$ Oe, jumps at T_c of Pb were observed; the large value of the specific heat jump $\Delta C/\gamma T_c \sim 1.4$ for the Pb regions (42% in molar ratio to Sn) is clearly greater than the value expected by weak-coupling BCS model[27] ($\Delta C/\gamma T_c = 1.43$), which is consistent with the strong-coupling nature of Pb and alloyed Pb[28]. Noticeably, the jump at T_c of Sn ($T \sim 3.7$ K) corresponding to the emergence of the superconducting states of Sn was observed only for the ZFC data, suggesting that the Sn regions do not undergo a *bulk* superconducting transition with a large entropy change after FC. Therefore, the trapped fluxes should be mainly present in the Sn regions. We did not observe a clear decrease in the amount of FC magnetization until after at least two days, as shown in Supplementary Fig. 6, which evidences strong trapping of fluxes and merit when using this phenomenon in applications.

Discussion

To explore the possibility of initializing (ON-to-OFF switching) κ using magnetic field control, we focused on the characteristic point of the B–H loop, as shown in Fig. 3e. Coming back from positive high H, B crosses the $H = 0$ Oe line with finite positive B. Then, B reaches zero at −470 Oe. Therefore, we investigated whether B can return to the origin (H, B) = (0 Oe, 0 G). Figure 5a shows the M-H loop when measuring M at $H = 0 \rightarrow 1500 \rightarrow 0 \rightarrow -470 \rightarrow 0$ Oe; orange arrows in Fig. 5a, b explain this field experience process. $4\pi M$ reaches the origin position of the loop, and the inner magnetic flux density B also reaches its origin, as shown in Fig. 5b. These results indicate that certain magnetic-field controls can return net B to the initial value. We expected a reduction in κ due to the recovery of superconductivity of the Sn regions using the same magnetic field control, but, as shown in Fig. 5c–e, κ does not reach the initial value. Those results imply the absence of bulk superconductivity in the Sn regions even in the state of net $B = 0$ G achieved after the process of $H = 0 \rightarrow 1500 \rightarrow 0 \rightarrow -470 \rightarrow 0$ Oe. From the results on net B and κ, we concluded that local B does not become zero, where the compensation of fluxes parallel to $+H$ and $-H$ resulted in net $B = 0$ G. Although we have not directly measured the direction of trapped fluxes (and/or vortices) of the solder, the coexistence of fluxes with opposite directions can be assumed from the results. As magnetic field control cannot achieve initialization of κ in the solders, other methods should be developed to achieve nonvolatile MTS with initialization functionality. Heating up to $T > T_c$ ($T > 7.2$ K for the solder) or flowing current greater than the critical current density will work to reset the flux-trapping states and initialize the κ value, because of breaking the superconducting states. In Fig. 5f, the temperature evolution of κ measured at $H = 0$ Oe after FC (1500 Oe) is shown. The initialization of κ by increasing the sample temperature to $T > T_c$ is achieved.

To further obtain experimental proofs for the flux trapping in the Sn regions, we performed magneto-optical (MO) imaging for the Sn45–Pb55 solder at $T = 2.5$ K. The obtained images are shown in Supplementary Fig. 7. Image (i) corresponds to the initial state after ZFC where no magnetic flux is trapped. When the magnetic field is $H = 1500$ Oe, greater than the critical field of the solder, μm-order structures are observed in image (ii). These structures indicate the uniform presence of magnetic fluxes in the normal conducting states. After decreasing H to 0 Oe, magnetic fluxes are expelled from the Pb regions and trapped in the Sn regions only. In image (iii), we observe blurriness of the structures and the emergence of contrast different from image (ii). By applying negative H, reversed trends are seen. In image

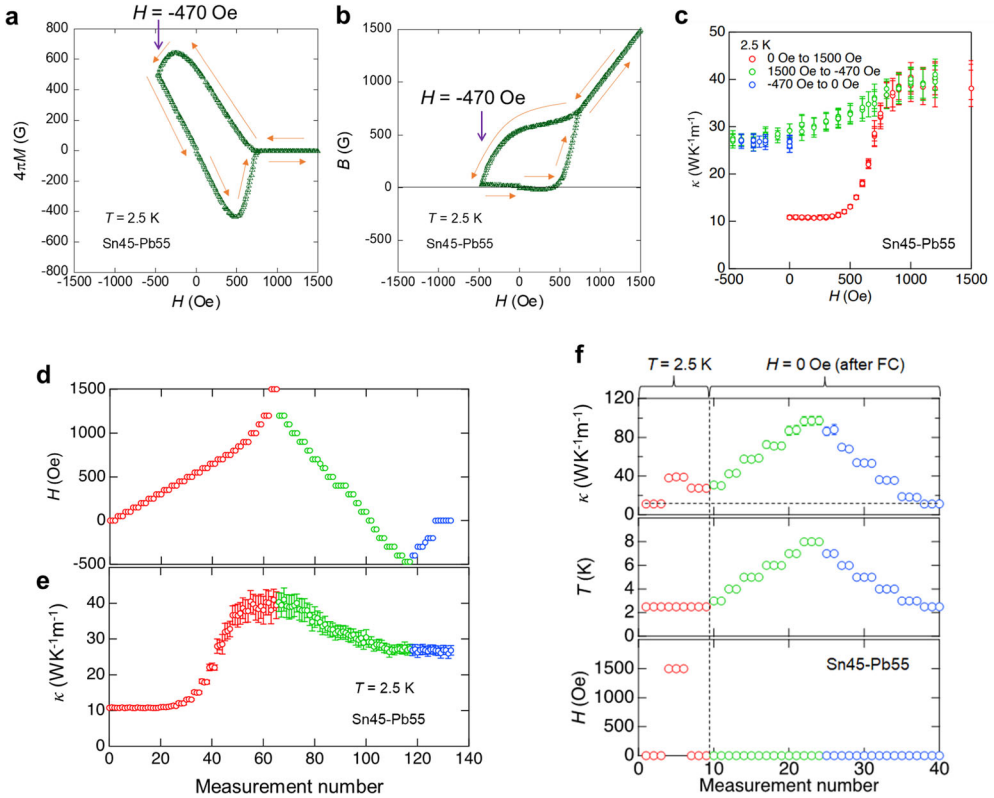

Fig. 5 | Minor loop measurements and initialization of κ. a, **b** H dependence of $4\pi M$ and B at $T = 2.5$ K for the solder (Sn45–Pb55), measured when H was swept between 1500 Oe and −470 Oe. See the arrows for the guide for measurement order. **c**, H dependence of κ, measured when H was swept from 0 to 1500 Oe (red), from 1500 to −470 Oe (green), and from −470 to 0 Oe (blue). It is clearly shown that the initial κ cannot be recovered by any magnetic-field control. **d**, **e** Measurement number dependence of H and κ at $T = 2.5$ K, extracted from the data in (**c**). **f** Initialization of κ by heating the sample above T_c. Measurement number dependence of κ, T and H. First, the ON state was produced by applying $H = 1500$ Oe and reducing the field to zero at $T = 2.5$ K (measurement number: 1–9). For numbers 10–24, temperature was gradually increased to $T = 8.0$ K. Then, temperature decreased to $T = 2.5$ K for numbers 25–40, and the initial κ is recovered as indicated by the dashed line.

(iii), the light parts would be Pb-rich regions, and the dark parts would be Sn-rich regions. Because of the inhomogeneous distribution of Sn regions, we just observed the blurriness and the changes in contrast. If magnetic fluxes are trapped at the grain boundaries, the MO image should show a uniform image in the flux-trapping states. Therefore, the present results can exclude the scenario of trapping at the grain boundaries. To obtain further evidence of the magnetic fluxes in the Sn regions, investigation with other techniques is needed to directly observe trapped fluxes in the solders.

For the future application of this phenomenon, the tunability of nonvolatile MTS is preferred. Here, we investigated the Sn-content dependence of nonvolatile MTS (Supplementary Fig. 8). For Sn90-Pb10, clear nonvolatility is not observed, but for Sn10-Pb90, nonvolatile MTS of ~ 300% is observed. In addition, the κ values change with changing Sn amount. Furthermore, we evaluated minor-loop characteristics of κ-H for the Sn45–Pb55 solder (Supplementary Fig. 9). As shown in Supplementary Fig. 10i, nonvolatile MTS is determined by the maximum field. The tunability of nonvolatile MTS by composition and magnetic field provides new thermal management functionalities.

Here, we demonstrated that Sn–Pb solders exhibit nonvolatile MTS by utilizing the superconducting states of Pb and flux trapping in the Sn regions. In the solders, the coexistence of two superconducting phases with different T_c , $T_c = 7.2$ K for Pb and $T_c = 3.7$ K for Sn, gives rise to nonvolatile MTS based on the changes in κ_{el}. In addition, the trapped fluxes large enough to suppress bulk superconductivity of the Sn regions are essential for this phenomenon; hence, $B > H_c$ for Sn was the preferred condition in the present case. The concept that superconductor composites can work as nonvolatile MTS materials is quite simple and applicable to various pairs of superconductors. For example, using high-T_c superconductors in the nonvolatile MTS composite would increase the working temperature of the nonvolatile MTS phenomena by making a composite with metals, alloys, or intermetallic compounds. Optimizing phase-separation conditions should enhance the switching ratio and flexibility of nonvolatile MTS.

Furthermore, since the Sn–Pb solder is widely used in electrical wiring, the large nonvolatile thermal switching and magnetic flux trapping in the solders should significantly affect low-temperature transport measurement techniques that were believed to have already established. Therefore, understanding the magneto-transport phenomena in solders is essential for reliable transport measurements at low temperatures under magnetic fields.

Methods

Samples

We used commercial solders: flux-core-less Sn45–Pb55 solder wires (φ1.6 mm, TAIYO ELECTRIC IND. CO., LTD.) and flux-cored Sn60-Pb40 solder wires (φ0.8 mm, HOZAN). The data shown in the main text was taken on a polished sample of Sn45–Pb55 solder wire. The purity of the Sn45-Pb55 solder wire was investigated by X-ray Fluorescence (XRF), and the actual Sn ratio was confirmed as 43.84(2)% in the weight ratio and $Sn_{0.58}Pb_{0.42}$ in the molar ratio. The Cu impurity with a weight ratio of 0.2% was detected by XRF. The Sn10-Pb90 and Sn90-Pb10 solders with 99.9% purity were purchased from SASAKI SOLDER INDUSTRY CO., LTD.

Characterization

Scanning-electron microscope (SEM) and energy-dispersive X-ray spectroscopy (EDX) were used to analyze chemical compositions on the surface of the solders. The images for Sn45–Pb55 shown in the main text were taken using Carl Zeiss Cross-Beam 1540ESB and those for Sn60-Pb40 were taken

using TM3030 (Hitachi Hightech). XRF was performed using JSX-1000S (JEOL).

Physical property measurements

Thermal conductivity (κ) was measured by means of a Physical Property Measurement System (PPMS, Quantum Design) with a thermal transport option (TTO) using a four-probe steady-state method with heater, two thermometers, and base-temperature terminal. The lengths between two thermometers attached to the measured samples were 55.5 mm for the Sn45–Pb55 rectangular bar with a cross-section area of 0.88 × 1.10 mm^2 (reported in the main text), 65.0 mm for the Sn45–Pb55 wire with a φ1.6 mm in diameter (reported in Supplementary Fig. 3), and 44.5 mm for Sn60-Pb40 (reported in Supplementary Fig. 4). Due to the limitation of the sample-room space of the TTO stage, the sample was screwed to store inside with four probes, a heater, two thermometers, and thermal base. The typical measurement duration for a single measurement was 30 s. The main result (κ–H at 2.5 K) was measured manually (not in a sequence mode) to check the temperature stability and the reliability of the relaxation curves.

Magnetization was measured by a superconducting quantum interference device (SQUID) magnetometry on Magnetic Property Measurement System (MPMS3, Quantum Design) with a VSM mode. Specific heat was measured on PPMS by a relaxation mode. The sample was attached to a stage using APIEZON N grease. Electrical resistivity was measured on PPMS by a four-probe method under magnetic fields.

Magneto-optical imaging. For magneto-optical imaging, we used PPMS and an infinity-corrected objective lens inserted into the sample space by the microscope which is set above the PPMS at approximately 1 m from the sample position[29]. The images shown here were prepared by subtracting the images taken at T = 8.0 K (normal state) from those taken at T = 2.5 K and normalized by data taken at T = 8.0 K.

Data availability

All relevant data are available from the corresponding author upon reasonable request.

Received: 7 December 2023; Accepted: 26 February 2024;
Published online: 15 March 2024

References

1. Li, N. et al. Phononics: Manipulating heat flow with electronic analogs and beyond. *Rev. Mod. Phys.* **84**, 1045 (2012).
2. Wehmeyer, G., Yabuki, T., Monachon, C., Wu, J. & Dames, C. Thermal diodes, regulators, and switches: physical mechanisms and potential applications. *Appl. Phys. Rev.* **4**, 041304 (2017).
3. Nishimura, Y. et al. Electronic and lattice thermal conductivity switching by 3D−2D crystal structure transition in nonequilibrium $(Pb_{1-x}Sn_x)Se$. *Adv. Electron. Mater.* **8**, 2200024 (2022).
4. Cho, J. et al. Electrochemically tunable thermal conductivity of lithium cobalt oxide. *Nat. Commun.* **5**, 4035 (2014).
5. Ihlefeld, J. F. et al. Room-temperature voltage tunable phonon thermal conductivity via reconfigurable interfaces in ferroelectric thin films. *Nano Lett.* **15**, 1791 (2015).
6. Kimling, J., Gooth, J. & Nielsch, K. Anisotropic magnetothermal resistance in Ni nanowires. *Phys. Rev. B* **87**, 094409 (2013).
7. Nakayama, H. et al. Above-room-temperature giant thermal conductivity switching in spintronic multilayer. *Appl. Phys. Lett.* **118**, 042409 (2021).
8. Kimling, J. et al. Spin-dependent thermal transport perpendicular to the planes of Co/Cu multilayers. *Phys. Rev. B* **91**, 144405 (2015).
9. Yoshida, M., Kasem, Md. R., Yamashita, A., Uchida, K. & Mizuguchi, Y. Magneto-thermal-switching properties of superconducting Nb. *Appl. Phys. Express* **16**, 033002 (2023).
10. Yoshida, M., Arima, H., Yamashita, A., Uchida, K. & Mizuguchi, Y. Large magneto-thermal-switching ratio in superconducting Pb wires. *J. Appl. Phys.* **134**, 065102 (2023).
11. Huang, H. L., Wu, D., Fan, D. & Zhu, X. Superconducting quantum computing: a review. *Sci. China Info. Sci.* **63**, 180501 (2020).
12. Kjaergaard, M. et al. Superconducting qubits: current state of play. *Annu. Rev. Condens. Matter Phys.* **11**, 369–395 (2020).
13. Kes, P. H., van der Veeken, J. P. M. & de Kierk, D. Thermal conductivity of niobium in the mixed state. *J. Low Temp. Phys.* **18**, 355 (1975).
14. Livingston, J. D. Magnetic properties of superconducting lead-base alloys. *Phys. Rev.* **129**, 1943–1949 (1963).
15. Furuya, S., Tominaga, A. & Narahara, Y. The wall-thickness dependence of magnetic shielding or trapping in a low-field superconductor, $Pb_{40}Sn_{60}$. *J. Low Temp. Phys.* **53**, 477–485 (1983).
16. Abrikosov, A. A. Nobel Lecture: Type-II superconductors and the vortex lattice. *Rev. Mod. Phys.* **76**, 975–979 (2004).
17. Harada, K. et al. Real-time observation of vortex lattices in a superconductor by electron microscopy. *Nature* **360**, 51–53 (1992).
18. Hess, H. F., Robinson, R. B. & Waszczak, J. V. STM spectroscopy of vortex cores and the flux lattice. *Physica B* **169**, 422–431 (1991).
19. Wells, F. S., Pan, A. V., Wang, X. R., Fedoseev, S. A. & Hilgenkamp, H. Analysis of low-field isotropic vortex glass containing vortex groups in $YBa_2Cu_3O_{7-x}$ thin films visualized by scanning SQUID microscopy. *Sci. Rep.* **5**, 8677 (2015).
20. Iguchi, Y. et al. Superconducting vortices carrying a temperature-dependent fraction of the flux quantum. *Science* **380**, 1244–1247 (2023).
21. Dolan, G. J. & Silcox, J. Critical thicknesses in superconducting thin films. *Phys. Rev. Lett.* **30**, 603–606 (1973).
22. Ge, J., Gutierrez, J., Cuppens, J. & Moshchalkov, V. V. Observation of single flux quantum vortices in the intermediate state of a type-I superconducting film. *Phys. Rev. B* **88**, 174503 (2013).
23. Doll, R. & Näbauer, M. Experimental proof of magnetic flux quantization in a superconducting ring. *Phys. Rev. Lett.* **7**, 51–52 (1961).
24. Minkov, V. S., Ksenofontov, V., Bud'ko, S. L., Talantsev, E. F. & Eremets, M. I. Magnetic flux trapping in hydrogen-rich high-temperature superconductors. *Nat. Phys*. https://doi.org/10.1038/s41567-023-02089-1 (2023).
25. Xing, X. et al. Anisotropic Ginzburg–Landau scaling of H_{c2} and transport properties of 112-type $Ca_{0.8}La_{0.2}Fe_{0.98}Co_{0.02}As_2$ single crystal. *Supercond. Sci. Technol.* **29**, 055005 (2016).
26. Stewart, G. R. Measurement of low-temperature specific heat. *Rev. Sci. Instrum.* **54**, 1–11 (1983).
27. Bardeen, J., Cooper, L. N. & Schrieffer, J. R. Theory of superconductivity. *Phys. Rev.* **108**, 1175–1204 (1957).
28. Padamsee, H., Neighbor, J. E. & Shiffman, C. A. Quasiparticle phenomenology for thermodynamics of strong-coupling superconductors. *J. Low Temp. Phys.* **12**, 387–411 (1973).
29. Kinoshita, Y., Miyakawa, T., Xu, X. & Tokunaga, M. Long-distance polarizing microscope system combined with solenoid-type magnet for microscopy and simultaneous measurement of physical parameters. *Rev. Sci. Instrum.* **93**, 073702 (2022).

Acknowledgements

The authors thank O. Miura, A. Yamashita, M. Yoshida, T. D. Matsuda, K. Hattori, R. Kurita, Y. Oikawa, H. Fujihisa, A. Kikkawa, and T. Machida for support in experiments and fruitful discussion on the results. This work was partly supported by JST-ERATO (JPMJER2201), TMU Research Project for Emergent Future Society, the joint research in the Institute for Solid State Physics, the University of Tokyo (202306-HMBXX-0090), and Tokyo Government Advanced Research (H31-1).

Author contributions

K.U. and Y.M. planned and supervised the study. H.A., H.S.A., K.U., Y.K., M.T., and Y.M. designed the experiments. H.A., M.R.K., H.S.A., Y.K., M.T., and Y.M. collected and analyzed the data. H.A., F.A., K.U., and Y.M. prepared the manuscript. All the authors discussed the results, developed an explanation of the experiments, and commented on the manuscript.

Competing interests

The authors declare no competing interests.

Additional information

Supplementary information The online version contains supplementary material available at https://doi.org/10.1038/s43246-024-00465-9.

Correspondence and requests for materials should be addressed to Yoshikazu Mizuguchi.

Peer review information *Communications Materials* thanks the anonymous reviewers for their contribution to the peer review of this work. Primary Handling Editor: Aldo Isidori.